Serrated flow behavior induced by blunt mechanism of shear crack propagation in metallic glass

J.T. Fan[a)] and Z.F. Zhang[b)]
Shenyang National Laboratory for Materials Science, Institute of Metal Research,
Chinese Academy of Sciences, Shenyang 110016, People's Republic of China

S.X. Mao
Shenyang National Laboratory for Materials Science, Institute of Metal Research, Chinese Academy
of Sciences, Shenyang 110016, People's Republic of China; and Department of Mechanical
Engineering, University of Pittsburgh, Pittsburgh, Pennsylvania 15261

B.L. Shen
Ningbo Institute of Materials Technology and Engineering, Chinese Academy of Sciences,
Ningbo, 315201, People's Republic of China

J. Eckert[c)]
IFW Dresden, Institut für Komplexe Materialien, D-01171 Dresden, Germany; and Technische
Universität Dresden, Institute of Materials Science, D-01062 Dresden, Germany

We present a blunt mechanism to explain the serrated flow behavior and slight "work hardening" at the beginning of yielding during the compression of metallic glass, which is in line with the piling-up of parallel shear bands on the fracture surface with a gradually increasing space from the edge of surface to inside. Meanwhile, two intrinsic parameters, i.e., strength intensity of blunt behavior, K, and global work-hardening sensitivity exponent, n, are introduced to characterize the blunt effect on the net increase in flow stress or work-hardening behavior of metallic glass.

I. INTRODUCTION

Because the unique plastic deformation in bulk metallic glasses (BMGs) is only confined to the localized narrow regions (called shear bands and characterized by the excess free volume),[1,2] shear bands become a close, concerned subject and eternal problem to be investigated.[1–3] Transmission electron microscope (TEM) observations on shear bands showed that the thickness of shear bands is in the range of 10 to 60 nm, depending on the testing conditions.[3] In a recent study, Li et al.[4] observed some nanometer scale voids within the shear bands, correlated with the coalescence of excess free volume following the plastic flow, with quantitative high-resolution transmission electron microscope (HRTEM). In addition, the deformation-induced in situ nanocrystallization was observed by HRTEM to further block plastic flow along some shear bands.[5] Moreover, many investigations indicate that the formation of shear bands was affected by the ambient temperature, stress state, annealing condition, sample geometry, second phase, particle or fiber, and so on, which led to the different deformation and fracture behavior.[6–10] Zhang and Eckert[11] proposed the unified tensile fracture criterion to soundly explain the observed three different failure modes of BMGs.[12] In addition, a fracture mode factor $\alpha = \tau_0/\sigma_0$[11] and fragmentation coefficient, F_n ($F_n = A_n/A_0$),[13] were defined to describe the different deformation and fracture behaviors of various BMGs. However, despite the extensive work that was devoted to elucidate the theories on the deformation and fracture behaviors of BMGs, the intrinsic character of shear bands is still under debate,[14] and there is no clear understanding of the role that shear bands play in the plasticity of BMGs. In this study, we report a blunt mechanism during shear crack propagation, which contributed to the serrated flow behavior and slight "work hardening" during the compression of BMGs.

II. EXPERIMENTAL

The $Zr_{55}Cu_{30}Al_{10}Ni_5$ alloy used in our research was prepared with the high pure (5N) constituents and was cast into a Cu mold in a high pure argon atmosphere with a diameter of 3 mm using an arc-melting apparatus (NISSIN GIKEN type NEV-ACH3) after remelting for

Address all correspondence to these authors:
[a)]e-mail: jtfan@imr.ac.cn
[b)]e-mail: zhfzhang@imr.ac.cn

several times.[15] The final ingot was analyzed by x-ray diffraction (XRD) using a Rigaku diffractometer with Cu-radiation as a source. The result shows that the alloy is a fully amorphous structure without any crystalline phase. The uniaxial compressive test was conducted on the BMG samples having dimensions of $\Phi 3$ mm $\times$ 6 mm with a computed-controlled, servo-hydraulic INSTRON-8801 testing machine with the extensometer in a strain rate of $1 \times 10^{-4} \text{s}^{-1}$ at room temperature. Finally, all of the deformation and fracture morphologies were observed by using a Quanta-600 scanning electron microscope (SEM; FEI, Eindhoven, The Netherlands).

III. RESULTS AND DISCUSSIONS

Figure 1(a) shows the compressive engineering stress-strain curve of the $Zr_{55}Cu_{30}Al_{10}Ni_5$ alloy. Its yield strength, $\sigma_{0.2}$, fracture strength, σ_b, and compressive plastic strain, ε_p, are approximately 1.75 GPa, 1.98 GPa, and 3.3%, respectively. Once the BMG sample started to yield, its flow stress displayed a serrated fluctuation, simi-lar to a previous report.[16] Visibly, the stress fluctuation amplitude (SFA) is very small at the beginning, but the stress-increasing amplitude (SIA), σ_I, is always higher than the stress-decreasing amplitude (SDA), σ_D, leading to a local work-hardening behavior at the beginning of yielding in the stress-strain curve, indicated as region A and the amplified photo in the inset of Fig. 1(b). Then, the SFA becomes larger and larger, but the SDA, σ_D, is approximately equal to the SIA, σ_I, with a value of 60 MPa. With further deformation, the total tendency of stress-strain curve keeps horizontal without global work-hardening behavior, as indicated by region B in [Fig. 1(a)]. However, some serrated flows with low stress fluctuation appear during the stress fluctuation, as indicated by the arrows in Fig. 1(a), with a stress fluctuation range from 20 to 50 MPa. This result implies that the disappearance of global work hardening is mainly due to the increase in the SDA. Then, the SFA suddenly rises up to approximately 180 MPa, approximately three times greater than that in region B. Finally, the BMG sample failed catastrophically with the speedy crack propagation, which is defined as region C in [Fig. 1(a)]. The same, true stress-strain curve also shows the slight working hardening at the beginning of yielding with the serrated flow behavior until the final fracture, as shown in the inset of Fig. 1(a). In summary, the BMG sample displayed certain work-hardening behavior at the beginning of yielding, and then plastically deformed with a serrated flow behavior, up to a plastic strain of 3.3%, and finally failed catastrophically with a speedy shear fracture.

Figure 2(a) clearly shows that the fracture occurs in a shear mode, and the compressive shear fracture angle, θ_c, between the stress axis and the fracture plane, is approximately 42°, according with the theoretical analysis by Zhang et al.[17] Further observations show that there are only a few straight shear bands, which are parallel to each other at a proportional space of approximately 270 µm, similar to a previous report.[18] The few shear bands seem to conflict with the plasticity of 3.3%.[19] Figure 2(b) shows that there is a wide shear step, approximately 300 µm, from the edge of surface with a characterless flat plane, just like the cement flooring. The further observations reveal that the characterless flat shear plane contains some visible ridge lines, which is in accordance with the shear direction, as indicated by the arrows in [Fig. 2(c)]. In addition, at some place, approximately 170 µm from the edge of fracture surface, many fine shear bands emerge from the flat shear plane, signed by the ellipse [Fig. 2(b)]. The amplified photo shows that the highly dense shear bands, with a small space of approximately 500 nm or less, are parallel to each other and perpendicular to the shear direction [Fig. 2(d)], which is similar to the report.[20] In addition, some vein-like structures were observed laying on the shear bands. In a word, at the beginning of shear deformation, the wide shear step
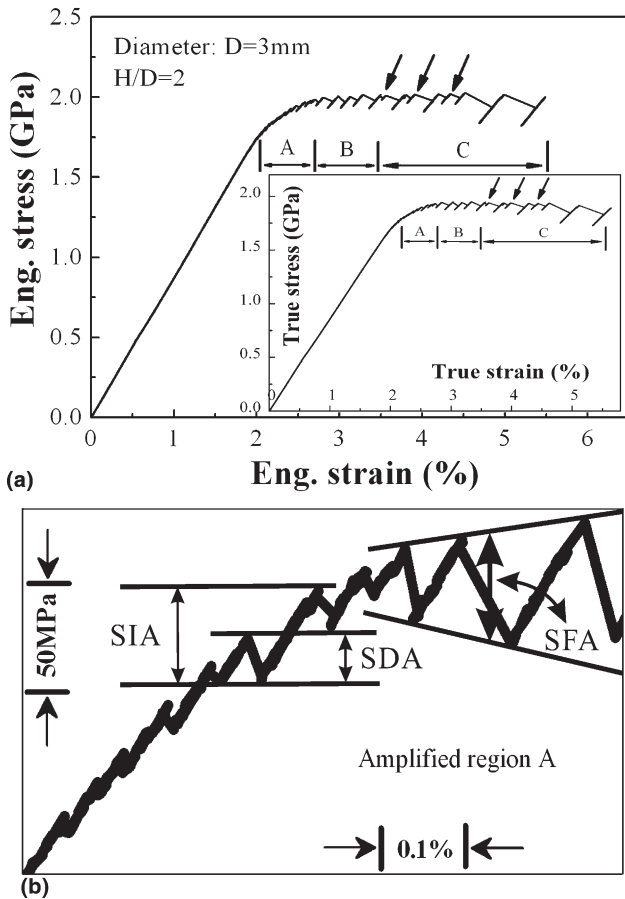

FIG. 1. (a) Compressive engineering stress-strain curve of $Zr_{55}Cu_{30}Al_{10}Ni_5$ amorphous alloy at a strain rate of $1 \times 10^{-4}\text{s}^{-1}$, divided into three regions A, B, and C, and the inset shows the corresponding true stress-strain curve; (b) amplified region A, indicating the stress fluctuation amplitude (SFA), stress-increasing amplitude (SIA), and stress-decreasing amplitude (SDA).
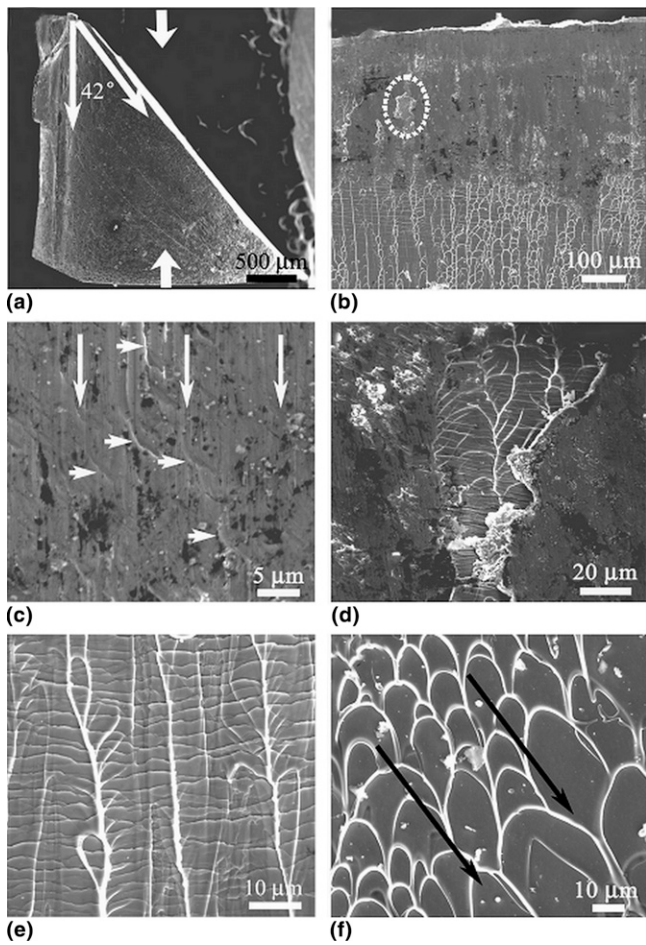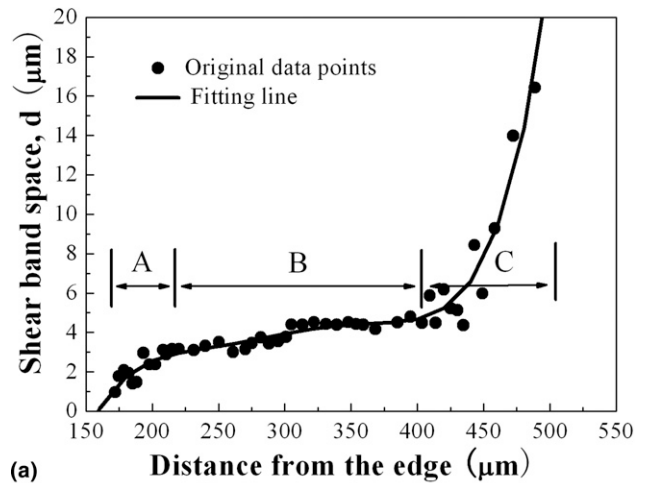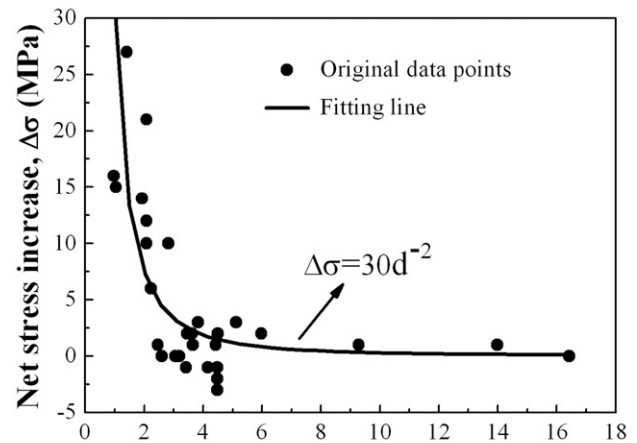
FIG. 2. SEM images of the fractographies of metallic glass after the compressive test: (a) the exterior surface with a few coarse primary shear bands; (b) the flat shear plane, vein-like structure and parallel shear bands; (c) the amplified characterless flat shear plane; (d) the highly dense shear bands; (e) the parallel shear bands below the vein-like structure; (f) the vein-like structure, implying a speedy crack propagation without any blunt behavior.

FIG. 3. (a) Quantitative analysis on the change of the shear band space, d, with the distance from the edge of fracture surface and its fitting curve; (b) the dependence of the net stress increase value, $\Delta\sigma$ on the shear band space, d, and its fitting curve with the algebraic equation.

is formed with the three layers: the bottom is shear bands; the middle is a vein-like pattern; and the top is the characterless flat shear plane. Thereinto, the bottom shear bands are normal to the direction of shear crack propagation and should result from the blunt behavior of the main shear crack. The middle vein-like pattern should be induced by the local melting within the shear band layer due to the release of high elastic energy during fracture.[21] The top characterless flat shear plane might be associated with the incompletely melting or the viscid flow in the brim of shear layer with a lower temperature rise.

On the other hand, it is found that the space between the parallel shear bands becomes bigger and bigger with the main shear crack propagation. The same, intact vein-like pattern vividly emerges above the shear bands, implying that the shear bands were formed before the vein-like pattern [Fig. 2(e)]. With continuous propagation of the main shear crack, the shear band space

suddenly becomes large and finally up to the maximum value of approximately 16.5 μm. Meanwhile, the parallel shear bands become distinct and trend to form the small crack, suggesting a gradually strong blunt behavior during shear crack propagation, which corresponds to the high SFA in region C in Fig. 1(a). In the end, the vein-like pattern spreads all over the rest of the fracture surface without any shear bands, implying a catastrophic failure without the blunt effect, as indicated by arrows in Fig. 2(f). The illumination above indicates that the shear band space increases with the increase in the distance from the edge. Figure 3(a) shows the dependence of the shear band space on the distance from the edge. It clearly shows that the curve can be divided into three different stages: i.e., regions A, B, and C, as signed in Fig. 3(a). Region A corresponds to the initiation of shear crack after yielding [Fig. 2(b)]. The initial global work-hardening behavior should result from the highly dense shear bands, triggered by the blunt behavior of

shear crack. With continuous deformation, the shear band space rises up, and then keeps at a constant level, approximately 3.5 μm [region B in Fig. 3(a)], which caused the gradually disappearance of global work-hardening behavior in this region. Finally, with further increases in the shear band space, the sharpening of crack becomes more and more serious, resulting in the finally catastrophic failure without global work-hardening behavior [region C in Fig. 3(a)].

From the analysis above, regions A, B, and C in Fig. 1(a) should be corresponding to regions A, B, and C in Fig. 3(a), respectively. Meanwhile, they are also in accord with the main shear crack propagation track [Figs. 2(d)–2(f)]. Figure 4(a) illuminates the formation and piling-up mechanism of the shear bands on the fracture surface, which were caused by the blunt effect. At the beginning of the main shear crack propagation, due to the strong blunt behavior, more shear bands were triggered and piled up at the edge of fracture surface, which led to the notable initial global work-hardening behavior, corresponding to region A in its stress-strain curve [Figs. 1(a) and 1(b)]. With the crack propagation, although the blunt behavior is still strong, the stress spurring the main shear crack propagation becomes larger due to the decrease in the effective contact area. Thus, the blunt behavior cannot offset the speedy crack propagation. Therefore, although the SFA is still large, there is no trace of global work-hardening behavior [regions B and C in Fig. 1(a)]. In addition, to explicitly illustrate the relationship between the density of shear bands and the work-hardening behavior, Fig. 4(b) shows the diagrammatic sketch of the evolving processes of fracture micrograph along the main shear crack propagation direction, together with the serrated flows in its stress-strain curve. Thus, the net increase in flow stress,

$\Delta\sigma$, is equal to the difference between the SIA, σ_I, and the SDA, σ_D, i.e.,

$$\Delta\sigma = \sigma_I - \sigma_D \quad . \qquad (1)$$

Meanwhile, we plotted a curve to show the net stress increase value, $\Delta\sigma$, and the shear band space on the fracture surface, d, as shown in Fig. 3(b). By fitting, it can be easily found that the net stress increase value, $\Delta\sigma$, reduces with the increase in the shear band space, d, with the following relationship:

$$\Delta\sigma = Kd^{-n} \quad , \qquad (2)$$

where K is named as the strength intensity of blunt behavior, and n is defined as the global work-hardening sensitivity exponent, both of which are intrinsic parameters to character the work-hardening ability. For the current case shown in Fig. 3(b), the calculated constants K and n are equal to approximately 30 ± 2 and 2 ± 0.05 MPa, respectively.

In addition, when the shear band space, d, is close to zero, i.e., $d \to 0$, the net stress increase value, $\Delta\sigma$, will be prone to ∞ and expressed as follows:

$$\lim_{d \to 0} \Delta\sigma = \infty \quad . \qquad (3)$$

This indicates that the intrinsic global work-hardening ability of metallic glass strongly depends on the shear band space. If the highly dense shear bands can be triggered, the global work-hardening ability can become strong. On the other hand, when the shear band space, d, is prone to ∞, i.e., $d \to \infty$, the net stress increase value, $\Delta\sigma$, will be close to 0, as expressed below:

$$\lim_{d \to \infty} \Delta\sigma = 0 \quad . \qquad (4)$$

The above expression demonstrates that when the shear band space, d, is too great, the net stress increase value, $\Delta\sigma$, will be prone to 0, indicating the disappearance of global work-hardening ability.

At the same time, the global work-hardening sensitivity exponent, n, is the rate of the change in net stress increase value, $\Delta\sigma$, with the shear band space, which reflects the sensitivity degree of local flow stress increase to the shear band space, d. In addition, it is an intrinsic parameter for the BMG materials, decided by the inherent factor. The smaller the n parameter, the stronger the work-hardening ability. In addition, the strength intensity of blunt behavior, K, is also an intrinsic parameter for metallic glass, which presents a comprehensive contribution of all the piling-up of shear bands to the net increase in flow stress. The greater the K parameter, the stronger the work-hardening ability. Therefore, higher K and lower n are beneficial to the improvement of global work-hardening ability, which can contribute to the toughness of metallic glasses with high strength and good plasticity.
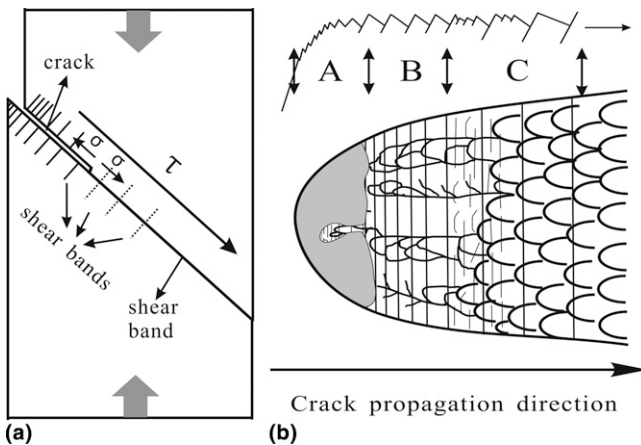

FIG. 4. Illustration of the main shear crack propagation process with the blunt behavior: (a) the formation and piled-up mechanism of local shear bands on the fracture surface; (b) the evolving process of shear plane, shear bands and vein-like structure, corresponding to the compressive engineering stress-strain curve.

IV. CONCLUSIONS

In summary, we observed some parallel shear bands on the fracture surface of metallic glass, when it was subjected to the quasistatic compression. By quantitative measurement and calculation, we found that the shear band space increased with the crack propagation, and the global work-hardening behavior became gradually slight or disappeared completely. It is considered that the global work-hardening behavior is associated with the piling-up mechanism of local shear bands during the crack propagation. Furthermore, two parameters, K and n, are introduced to characterize the global work-hardening ability of metallic glass. In principle, the higher strength intensity of blunt behavior, K, and lower global work-hardening sensitivity exponent, n, can lead to a higher global work-hardening ability, which contributes to the high toughness of metallic glass.

ACKNOWLEDGMENTS

REFERENCES

1. C.A. Pampillo: Flow and fracture in amorphous alloys. *J. Mater. Sci.* **10,** 1194 (1975).
2. F. Spaepen: A microscopic mechanism for steady state inhomogeneous flow in metallic glasses. *Acta Metall.* **25,** 407 (1977).
3. P.E. Donovan and W.M. Stobbs: The structure of shear bands in metallic glasses. *Acta Metall.* **29,** 1419 (1981).
4. J. Li, F. Spaepen, and T.C. Hufnagel: Nanometre-scale defects in shear bands in a metallic glass. *Philos. Mag. A* **82,** 2623 (2002).
5. M. Chen, A. Inoue, W. Zhang, and T. Sakurai: Extraordinary plasticity of ductile bulk metallic glasses. *Phys. Rev. Lett.* **96,** 245502 (2006).
6. X.L. Fu, Y. Li, and C.A. Schuh: Temperature, strain rate and reinforcement volume fraction dependence of plastic deformation in metallic glass matrix composites. *Acta Mater.* **55,** 3059 (2007).
7. F.H. Dalla Torre, A. Dubach, M.E. Siegrist, and J.F. Löffler: Negative strain rate sensitivity in bulk metallic glass and its similarities with the dynamic strain aging effect during deformation. *Appl. Phys. Lett.* **89,** 091918 (2006).
8. F.F. Wu, Z.F. Zhang, S.X. Mao, A. Peker, and J. Eckert: Effect of annealing temperature on the mechanical properties and fracture mechanisms of a $Zr_{56.2}Ti_{13.8}Nb_{5.0}Cu_{6.9}Ni_{5.6}Be_{12.5}$ bulk metallic glass composite. *Phys. Rev. B: Condens. Matter.* **75,** 134201 (2007).
9. Z.F. Zhang, H. Zhang, X.F. Pan, J. Das, and J. Eckert: Effect of aspect ratio on the compressive deformation and fracture behaviour of Zr-based bulk metallic glass. *Philos. Mag. Lett.* **85,** 513 (2005).
10. F. Szuecs, C.P. Kim, and W.L. Johnson: Mechanical properties of $Zr_{56.2}Ti_{13.8}Nb_{5.0}Cu_{6.9}Ni_{5.6}Be_{12.5}$ ductile phase reinforced bulk metallic glass composite. *Acta Mater.* **49,** 1507 (2001).
11. Z.F. Zhang and J. Eckert: Unified tensile fracture criterion. *Phys. Rev. Lett.* **94,** 094301 (2005).
12. Z.F. Zhang, G. He, J. Eckert, and L. Schultz: Fracture mechanisms in bulk metallic glassy materials. *Phys. Rev. Lett.* **91,** 045505 (2003).
13. Z.F. Zhang, H. Zhang, B.L. Shen, A. Inoue, and J. Eckert: Shear fracture and fragmentation mechanisms of bulk metallic glasses. *Philos. Mag. Lett.* **86,** 643 (2006).
14. K.M. Flores and R.H. Dauskardt: Fracture and deformation of bulk metallic glasses and their composites. *Intermetallics* **12,** 1025 (2004).
15. Y. Yokoyama, K. Yamano, K. Fukaura, H. Sunada, and A. Inoue: Ductility improvement of $Zr_{55}Cu_{30}Al_{10}Ni_5$ bulk amorphous alloy. *Scr. Mater.* **44,** 1529 (2001).
16. C.A. Schuh, A.C. Lund, and T.G. Nieh: New regime of homogeneous flow in the deformation map of metallic glasses: Elevated temperature nanoindentation experiments and mechanistic modeling. *Acta Mater.* **52,** 5879 (2004).
17. Z.F. Zhang, J. Eckert, and L. Schultz: Difference in compressive and tensile fracture mechanisms of $Zr_{59}Cu_{20}Al_{10}Ni_8Ti_3$ bulk metallic glass. *Acta Mater.* **51,** 1167 (2003).
18. J.T. Fan, F.F. Wu, Z.F. Zhang, F. Jiang, J. Sun, and S.X. Mao: Effect of microstructures on the compressive deformation and fracture behaviors of $Zr_{47}Cu_{46}Al_7$ bulk metallic glass composites. *J. Non-Cryst. Solids* **353,** 4707 (2007).
19. H. Bei, S. Xie, and E.P. George: Softening caused by profuse shear banding in a bulk metallic glass. *Phys. Rev. Lett.* **96,** 105503 (2006).
20. Z.F. Zhang, J. Eckert, and L. Schultz: Fatigue and fracture behavior of bulk metallic glass. *Metall. Mater. Trans. A* **35,** 3489 (2004).
21. W.J. Wright, R. Saha, and W.D. Nix: Deformation mechanisms of the $Zr_{40}Ti_{14}Ni_{10}Cu_{12}Be_{24}$ bulk metallic glass. *Mater. Trans.* **42,** 642 (2001).

440

J. Mater. Res., Vol. 24, No. 2, Feb 2009